Neutron Capture and Total Cross-Section Measurements and Resonance Parameters of Gadolinium

Article *in* Nuclear science and engineering: the journal of the American Nuclear Society · November 2006

DOI: 10.13182/NSE05-64

10 authors, including:

Gregory Leinweber
Bechtel Marine Propulsion Corporation
45 PUBLICATIONS **124** CITATIONS
SEE PROFILE

Devin P Barry
Rensselaer Polytechnic Institute
43 PUBLICATIONS **137** CITATIONS
SEE PROFILE

Robert Block
Rensselaer Polytechnic Institute
281 PUBLICATIONS **2,606** CITATIONS
SEE PROFILE

Yaron Danon
Rensselaer Polytechnic Institute
197 PUBLICATIONS **1,452** CITATIONS
SEE PROFILE

NUCLEAR SCIENCE AND ENGINEERING: **154**, 261–279 (2006)

Neutron Capture and Total Cross-Section Measurements and Resonance Parameters of Gadolinium

G. Leinweber,* D. P. Barry, M. J. Trbovich, J. A. Burke, N. J. Drindak, H. D. Knox, and R. V. Ballad

Lockheed Martin Corporation
P.O. Box 1072, Schenectady, New York 12301-1072

and

R. C. Block, Y. Danon, and L. I. Severnyak

Rensselaer Polytechnic Institute
Department of Mechanical, Aerospace, and Nuclear Engineering
Troy, New York 12180-3590

Received July 28, 2005
Accepted December 20, 2005

Abstract—*Neutron capture and transmission measurements were performed by the time-of-flight technique at the Rensselaer Polytechnic Institute linac facility using metallic and liquid Gd samples. The liquid samples were isotopically enriched in either ^{155}Gd or ^{157}Gd. The capture measurements were made at the 25-m flight station with a multiplicity-type capture detector, and the transmission measurements were performed at 15- and 25-m flight stations with ^{6}Li glass scintillation detectors. The multilevel R-matrix Bayesian code SAMMY was used to extract resonance parameters.*

Among the significant findings are the following. The neutron width of the largest resonance in Gd, at 0.032 eV in ^{157}Gd, has been measured to be (9 ± 1)% smaller than that given in ENDF/B-VI updated through release 8. The thermal (2200 m/s) capture cross section of ^{157}Gd has been measured to be 11% smaller than that calculated from ENDF. The other major thermal resonance, at 0.025 eV in ^{155}Gd, did not display a significant deviation from the thermal capture cross section given by ENDF.

In the epithermal region, the analysis provided here represents the most extensive to date. Twenty-eight new resonances are proposed, and other resonances previously identified in the literature have been revisited. The assignment of resonances within regions of complicated structure incorporated the observations of other researchers, particularly on the six occasions where ENDF resonances are recommended to be removed. The poor match of the ENDF parameters to the current data is significant, and substantial improvement to the understanding of gadolinium cross sections is presented, particularly above 180 eV where the ENDF resolved region for ^{155}Gd ends.

I. INTRODUCTION

The purpose of the present work is to measure the neutron cross sections of gadolinium accurately. Gadolinium has the highest thermal cross section of any natural element. Two large resonances exist slightly above thermal energy. The resonances are in ^{155}Gd and ^{157}Gd. Isotopically enriched ^{155}Gd and ^{157}Gd samples were prepared as liquid solutions with heavy water to produce uniform, thin samples. These thin samples were used in conjunction with elemental, natural metal samples.

A more detailed description of the present measurement and analysis is given in Ref. 1.

II. HISTORICAL REVIEW

A review of the prior measurements of Gd shows that the resonance parameters for the low-energy doublet (at ≈0.03 eV) in ENDF/B-VI (Ref. 2) updated

*E-mail: leinwg@rpi.edu

through release 8 are nearly identical to those of Møller et al.[3] The neutron width of the low-energy ^{155}Gd resonance and the radiation widths of both low-energy resonances come directly from the paper of Møller et al.,[3] while the ENDF value for the neutron width of the low-energy ^{157}Gd resonance is within 0.4% of the value given by Møller et al.[3]

In the region from 1.0 to 300.0 eV, most of the resonances occur in ^{155}Gd and ^{157}Gd. In these two isotopes, ENDF resonance parameters are based on a few experiments, particularly Mughabghab and Chrien,[4] Simpson,[5] and Fricke et al.[6] The other high-abundance isotopes, ^{158}Gd and ^{160}Gd, have few resonances, and their parameters come from Mughabghab and Chrien[4] and Rahn et al.[7] The minority isotopes are ^{152}Gd and ^{154}Gd. Gadolinium-152 has a natural abundance of 0.2%. Its parameters come from Anufriev et al.[8] and Macklin.[9] Gadolinium-154 has a natural abundance of 2.1%. Its resonance parameters come from Refs. 7 and 9.

Many other authors contributed observed resonance energies and/or spin assignments for resonances energies above 148 eV including Belyaev et al.,[10] Karzhavina et al.,[11,12] and Asghar et al.[13]

III. EXPERIMENTAL CONDITIONS

Table I gives some details of the experimental conditions including neutron targets, overlap filters, linac pulse repetition rate, flight path length, and channel widths. Descriptions of the detectors,[14,15] data acquisition,[14,16] and neutron-producing targets[17–19] used in these experiments are available in the references.

The neutron energy for a detected event is determined using the time-of-flight (TOF) technique. The overall dead time of the signal-processing electronics has been set at 1.125 μs for capture measurements and 0.6 μs for transmission measurements.[14]

Table II lists the isotopic content of the gadolinium samples used in the experiments. The purity of metal samples was 99.8%. The isotopic abundances of the elemental metal samples are taken from Ref. 20. The only significant contaminant in the metal samples was tantalum with a manufacturer-specified content of $<$0.1%. The liquid samples were prepared by dissolving enriched gadolinium oxide in D_2NO_3 and then diluting in 99.80% pure D_2O. The uncertainties in isotopic enrichment of liquid samples given in Table II were determined by mass spectroscopy. No evidence of contamination was observed in the liquid sample data.

Table III lists the thicknesses of the samples and the measurements made with these samples. The uncertainties in sample thickness for metal samples were propagated from multiple measurements of sample weight and diameter. The diameter measurements were the dominant component of the uncertainties. The uncertainties in sample thickness for liquid samples are larger than those of metals as shown in Table III. The method used to determine the effective thickness of a liquid consists of weighing the quantity of Gd_2O_3 necessary for 10 ml of $GdNO_3$ solution in a 10-ml flask. Then, a known weight of DNO_3 is added to dissolve the Gd_2O_3. Next, a known weight of D_2O is added to bring the volume to 10 ml. The concentration of Gd_2O_3 is the weight in grams divided by 10 ml. The weights are accurate to 0.001% for a 5-g sample. The accuracy of this method is limited by the accuracy of the volumetric flask, i.e., 0.2%. Each of the samples used is a further dilution of the stock solution, introducing a second 0.2% error. Subsequent to the gadolinium sample preparation, a second method was developed. It consists of preparing more of each solution than is required, so that part of the batch can be extracted with a precision (0.02 vol%) pipette, fired and weighed. Experience has shown that estimates of sample thickness from these two methods can differ by 2%. The second method is preferred since it measures the final product. Application of this second method to the current measurements would require destructively analyzing the liquid samples used in this measurement, which was not done. Therefore, the uncertainty in sample thickness for the liquid samples is $\leq$2%.

All metal samples were natural elemental gadolinium sealed inside aluminum sample cans. The thickness of aluminum on each of the front and rear faces of each sample was 0.38 mm (15 mils; 1 mil = 0.001 in.). The influence of these sample cans, as well as all background, was measured by including empty sample cans in the capture measurement. Background in transmission measurements is discussed in Sec. IV.B.

The liquid samples were enclosed in quartz cells. A drawing of the quartz cell is given in Fig. 1. The liquid samples were needed to measure the strong thermal

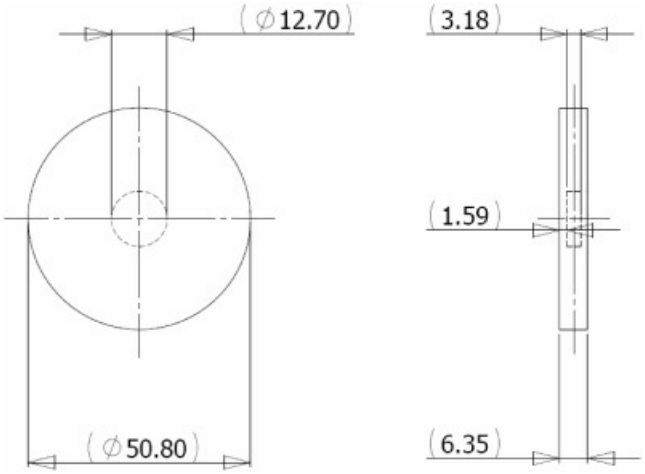

Fig. 1. Geometry of the quartz cells used for liquid samples for thermal measurements. Units are millimeter.

TABLE I

Gadolinium Experimental Details

Experiment	Overlap Filter	Neutron-Producing Target	Electron Pulse Width (ns)	Average Beam Current (μA)	Beam Energy (MeV)	Maximum Channel Width (μs)	Intermediate Channel Width (μs)	Minimum Channel Width (μs)	Pulse Repetition Rate (pulses/s)	Flight Path Length (m)
Epithermal transmission a	Boron carbide	Bare bounce	160	36	56	0.5 at <27 eV	0.125 at 27 to 236 eV	0.0625 at >236 eV	250	25
Epithermal transmission b	Cadmium	Bare bounce	153	40	50	0.5 at <27 eV	0.125 at 27 to 236 eV	0.0625 at >236 eV	250	25
Thermal transmission a enriched liquids	None	Enhanced thermal	1000	8	53	128 at <0.01 eV	32 at 0.01 to 0.04 eV 8 at 0.04 to 0.5 eV	0.5 at >0.5 eV	25	15
Thermal transmission b enriched liquids	None	Enhanced thermal	3000	19	60	256 at <0.008 eV	32 at 0.008 to 0.04 eV 8 at 0.04 to 0.19 eV	1.0 at >0.19 eV	25	15
Thermal transmission c natural (elemental) metals	None	Enhanced thermal	2100	8.5	50	8 at <0.29 eV	1 at 0.29 to 4.8 eV	0.5 at >4.8 eV	25	15
Epithermal capture	Cadmium	Bare bounce	128	45	58	2 at <1.5 eV	0.5 at 1.5 to 27 eV 0.125 at 27 to 236 eV	0.0625 at >236 eV	250	25
Thermal capture	None	Enhanced thermal	3280	19	52	2048 at <0.02 eV	128 at 0.02 to 0.06 eV 16 at 0.06 to 0.5 eV	1.0 at >0.5 eV	25	25

TABLE II

Liquid Gadolinium Isotopic Enrichment, Atom Percentages

	Samples	^{152}Gd	^{154}Gd	^{155}Gd	^{156}Gd	^{157}Gd	^{158}Gd	^{160}Gd
^{155}Gd: enriched	LX-1, LX-2, LX-4, LX-9	0.0108 ± 0.0002	0.9859 ± 0.0074	74.4233 ± 0.0095	17.5674 ± 0.0051	3.7513 ± 0.0023	2.5336 ± 0.0024	0.7278 ± 0.0020
^{157}Gd: enriched	LX-5, LX-6, LX-7, LX-10, LX-11	0.00510 ± 0.00004	0.07530 ± 0.00025	1.35147 ± 0.00070	7.3627 ± 0.0017	69.6623 ± 0.0081	19.4431 ± 0.0067	2.1000 ± 0.0015
Elemental metals		0.2	2.2	14.8	20.5	15.7	24.8	21.9

TABLE III

Elemental Metals and Liquid Isotopic Samples

Metal Samples	Gadolinium (atom/b)	Gadolinium Uncertainty (atom/b)	Measurements Included
0.025 mm (0.001 in.)	9.119E−05[a]	6E−08	Thermal and epithermal transmission 0.024 to 10 eV, and capture 1 to 300 eV
0.051 mm (0.002 in.)	1.713E−04	1E−07	Thermal and epithermal transmission 0.055 to 10 eV, and capture 1 to 300 eV
0.127 mm (0.005 in.)	4.127E−04	5E−07	Thermal and epithermal transmission 0.088 to 300 eV, and capture 1 to 300 eV
0.254 mm (0.010 in.)	7.806E−04	4E−07	Epithermal transmission 10 to 300 eV
0.508 mm (0.020 in.)	1.566E−03	5E−07	Epithermal transmission 10 to 300 eV
0.889 mm (0.035 in.)	2.886E−03	3E−06	Epithermal transmission 10 to 300 eV
1.27 mm (0.050 in.)	3.926E−03	2E−06	Epithermal transmission 10 to 300 eV
2.54 mm (0.100 in.)	8.070E−03	2.1E−05	Epithermal transmission and capture 10 to 300 eV
5.08 mm (0.200 in.)	1.577E−02	3E−05	Epithermal transmission 10 to 300 eV
1.02 cm (0.400 in.)	3.151E−02	6E−05	Epithermal transmission 10 to 300 eV
Liquid Samples	**Gadolinium (atom/b)**	**Gadolinium Uncertainty (atom/b)**	**Measurements Included**
LX-1	1.41E−04	≤2%[b]	Thermal transmission 0.047 to 1.0 eV
LX-2	4.58E−05	≤2%[b]	Thermal transmission 0.006 to 1.0 eV
LX-4	1.32E−05	≤2%[b]	Thermal transmission 0.002 to 1.0 eV, and thermal capture 0.01 to 1.0 eV
LX-5	1.27E−04	≤2%[b]	Thermal transmission 0.081 to 1.0 eV
LX-6	4.34E−05	≤2%[b]	Thermal transmission 0.046 to 1.0 eV
LX-7	1.19E−05	≤2%[b]	Thermal transmission 0.002 to 1.0 eV
LX-9	4.39E−06	≤2%[c]	Thermal capture 0.01 to 1.0 eV
LX-1	3.97E−06	≤2%[c]	Thermal capture 0.01 to 1.0 eV
LX-11	1.32E−06	≤2%[c]	Thermal capture 0.01 to 1.0 eV

[a]Read as 9.119×10^{-5}.

[b]In the chemical preparation of the liquid samples, the uncertainty in sample thickness is limited by the two required measurements of volume, each with an estimated uncertainty of 0.2%. The quadrature sum error is $\sqrt{(2x^2)} \approx 0.3\%$. However, thicknesses determined in this manner have been found to be discrepant by 2% (see Sec. VII.A).

[c]These three samples, LX-9, LX-10, and LX-11, were further diluted and therefore required a third measurement of volume with an uncertainty of 0.2%.

region doublet. The thinnest manufacturable metal sample of uniform thickness was 0.025-mm thickness. At this thickness the thermal region doublet is saturated. The liquid samples provided a uniform solution of enriched Gd in heavy water. The heavy water minimized non-Gd interactions. The sample container was a quartz cell with parallel inner walls. A D_2O blank in an equivalent quartz container was included in the liquid sample measurements as a background measurement.

III.A. Capture Detector

The capture detector is a gamma detector containing 20 ℓ of NaI(Tl) (Refs. 14, 15, and 16). The scintillation crystals form an annulus around the neutron beam with the sample at its center. The metal samples were 5.08 cm in diameter, and the neutron beam was collimated to 4.76 cm. Neutrons that scatter from the sample are absorbed by a hollow cylindrical liner fabricated of boron carbide ceramic to reduce the number of scattered neutrons reaching the detector. The liner uses boron enriched to 98.4 wt% ^{10}B for maximum neutron absorption. The liquid samples were 1.27 cm in diameter, and the neutron beam was collimated to 1.11 cm. The final collimator used for the liquid sample measurements was an annular cylinder of ^{10}B powder placed inside the detector just a few centimeters from the samples. The detector system discriminates against the 478-keV gamma ray from $^{10}B(n,\alpha)$ reactions. The efficiency of the capture detector is assumed to be the same for all Gd isotopes. Reference 14 contains a description of the detector and its signal-processing electronics.

III.B. Transmission Detectors

Neutron transmission measurements were conducted at the 15- and 25-m flight stations. The 15-m station contains a 7.62-cm (3-in.)-diam, 0.3-cm-thick NE 905 ^{6}Li glass scintillation detector (6.6% lithium, enriched to 95% in ^{6}Li) and is used for measurements covering the energy range from 0.002 to 10 eV. The 25-m station contains a 12.70-cm (5-in.)-diam, 1.27-cm-thick NE 905 ^{6}Li glass detector and covers the range from 1 to 300 eV. Each detector is coupled to a photomultiplier tube.

Transmission samples along with empty sample holders, which are used to measure the open-beam count rate, are mounted on an eight-position computer-controlled sample changer. The transmission function, which is approximately the ratio of the count rate with a sample in the beam to the count rate with samples removed, varies with neutron energy. Each data run consists of one complete cycle through the samples, with a predetermined number of linac bursts for each sample position. The distribution of bursts per sample position is chosen to minimize the counting statistical error in the measured cross section.[21]

IV. DATA REDUCTION

IV.A. Capture Data

Neutron capture data taking and data reduction techniques at the Rensselaer Polytechnic Institute (RPI) linac are described in Refs. 22 and 23.

For the thermal measurement of liquid samples, background was determined using a cell containing D_2O. For the epithermal measurement of metal samples, background was determined using empty aluminum sample cans.

Processed capture data are expressed as yield. Yield is defined as the number of neutron captures per neutron incident on the sample. Therefore, in addition to the sample data, another set of data was needed to determine the energy profile of the neutron flux. This was done by mounting a thick $^{10}B_4C$ sample in the sample changer and adjusting the total energy threshold to record the 478-keV gamma rays from neutron absorption in ^{10}B. The boron absorption spectrum provides an accurate representation of the energy profile of the linac's neutron beam flux convoluted with the $1/v$ boron (n,α) cross section. These flux data give the shape of the neutron beam flux but not its magnitude. The thermal flux was smoothed using a cubic spline interpolation. The thermal yield was normalized to the transmission data in a combined SAMMY fit. The epithermal flux was normalized to the black 6.3-eV predominantly-capture resonance in Gd. A small correction (1.8%) was made for the scattering in the 6.3-eV normalizing resonance. The 2.54-mm (100-mil) sample data were used for this normalization.

The zero time for each experiment was determined by performing a "gamma flash" measurement. The burst of gamma rays accompanying the neutron burst is detected by the capture detector. The centroid of the gamma-flash peak, less the time for light to travel the length of the flight path, is defined as the zero time of neutron production.

Finally, Y_i, the capture yield in TOF channel i, was calculated by

$$Y_i = \frac{C_i - B_i}{K\phi_i} \quad , \tag{1}$$

where

C_i = dead-time–corrected and monitor-normalized counting rate of the sample measurement

B_i = dead-time–corrected and monitor-normalized background counting rate

K = product of the flux normalization factor and efficiency

Φ_i = unnormalized neutron flux.

It was this capture yield and its associated statistical uncertainty that provided input to the SAMMY data analysis code[24] that extracted the neutron resonance parameters.

Four liquid capture samples were used in the analysis of the thermal region. The low-energy cutoff for capture data in the thermal region was 0.01 eV. Four natural metal samples were used in the epithermal region, 1 to 300 eV.

The flux-to-background ratio in the liquid sample thermal capture experiment peaked at approximately 35-to-1 at 0.1 eV, is 20-to-1 at the thermal region doublet, and fell to 3-to-1 at 0.01 eV. Capture data were not used below 0.01 eV The flux-to-background ratio for the natural metal epithermal capture experiment was approximately 400-to-1 from 150 to 300 eV and fell steadily to 300-to-1 at 40 eV, to 200-to-1 at 10 eV, and 80-to-1 at 2 eV.

IV.B. Transmission Data

For the thermal measurement, liquid sample cells containing D_2O were used as the open beam measurement. In this way the effect of the D_2O and quartz in the sample and open cells would cancel in transmission.

The time-dependent background was obtained with the one-notch/two-notch method.[25] The transmission function was calculated from Eq. (2):

$$T_i = \frac{(C_i^S - K_S B_i - B_S)}{(C_i^O - K_O B_i - B_O)} \quad , \tag{2}$$

where

T_i = transmission in TOF channel i

C_i^S, C_i^O = dead-time–corrected and monitor-normalized counting rates of the sample and open measurements, respectively

B_i = time-dependent background counting rate

B_S, B_O = steady-state background counting rates for sample and open measurements, respectively

K_S, K_O = normalization factors for the sample and open background measurements, respectively.

The backgrounds of the two thermal liquid sample measurements were normalized to extrapolated notch data in Cd at 0.15 eV.

Correction factors of up to 1.3% were applied to LX-1, LX-5, and LX-6 thermal transmission data due to sample misalignment, so that their transmissions went to zero in the saturated low-energy region.

For the thermal metal measurement, a single exponential function was used to interpolate between two known background points: a fixed indium notch at 1.4 eV and the region below 0.01 eV, where all metal Gd samples are black. Normalization constants K_S and K_O were fixed at 1.0 for the thermal metal measurement. Each sample's background function was calculated individually.

The background of the first epithermal measurement was normalized to the extrapolated notch in silver at 5.2 eV for all samples except the 1.02-cm (400-mil) sample, which was normalized at the saturated 20.5-eV resonance in Gd.

The background of the second epithermal measurement was normalized to the extrapolated notch in tungsten at 18.8 eV.

The epithermal flight path length (≈25.6 m) and zero time were fitted to match the energies from epithermal capture data.

Seven liquid transmission data sets were used in the thermal analysis. Three natural metal samples were used in the thermal and epithermal energy ranges up to 10 eV. Eleven additional natural metal transmission data sets were used in the epithermal analysis from 1 to 300 eV.

The signal-to-background ratios for the two liquid sample thermal experiments peaked at 2000-to-1 near 0.5 eV. The ratio in the region of the two strong thermal resonances in Gd was 1000-to-1. Signal-to-background fell to 10-to-1 at 2 meV, the lowest energy at which data were used. Signal-to-background ratios for the metal sample thermal experiment was 1000-to-1 or greater from thermal energies through 0.1 eV with a peak value of 2000-to-1 at 0.06 eV. The ratio fell to 200-to-1 at 0.5 eV and remained steady at 200-to-1 out to 10 eV. Signal-to-background ratios for the two metal sample epithermal experiments were rather constant with energy at approximately 45-to-1 for the boron-filtered experiment and approximately 75-to-1 for the cadmium-filtered experiment.

V. ANALYSIS METHODS

Resonance parameters, neutron width Γ_n, radiation width Γ_γ, and resonance energy E_0, were extracted from the capture and transmission data sets using the SAMMY version M6 multilevel R-matrix Bayesian code.[24] This was a combined transmission and capture analysis, which employed the resolution broadening, self-shielding, multiple-scattering, and diluent features of SAMMY. The present measurements assumed the same spin assignments as ENDF for all resonances analyzed.

In the liquid thermal capture measurement, a D_2O-only "blank" cell was used to measure background. The data were processed by subtracting the blank from the Gd plus D_2O capture data. The SAMMY geometry consists of a homogeneous mixture of Gd and D_2O. The three-dimensional geometry in MCNP (Ref. 26) allowed a realistic treatment of the neutron scattering and capture in Gd, D_2O, and the quartz cells. The resulting correction factors were applied to the liquid capture yield data. The factors ranged from 1.02 at 0.01 eV to 0.995 at 0.1 eV. They accounted primarily for quartz scattering and subsequent capture in Gd, which could not be modeled in SAMMY. More details are provided in Ref. 1.

For liquid thermal transmission analysis, no diluent, i.e., D_2O, specifications are needed. That is because D_2O-only blank cells are used for the open beam measurement, and therefore, the effect of the diluent cancels experimentally from the transmission, defined as (quartz + sample + diluent)/(quartz + diluent-only open beam). Therefore, the SAMMY model includes only Gd. The presence of Gd in the samples is so dilute that there is no need to account for D_2O displaced by the Gd.

The following assumptions were made for the SAMMY analysis:

1. Background was not fitted during the SAMMY analysis, which determined the final resonance parameters. Background was only varied in transmission in the 10- to 80-eV region as a sensitivity study for the purpose of determining uncertainties.

2. Resonance parameters of the two bound level resonances of Gd (^{152}Gd and ^{154}Gd) were not varied.

3. Resonance parameters of ^{152}Gd were not varied because of its low abundance (0.2%). They were fixed to ENDF values.

4. Normalization of the liquid sample thermal capture data was varied within a combined capture and transmission SAMMY fit.

5. Normalization was not varied for either capture or transmission in the epithermal region.

6. Energy regions over which each sample has been fitted are given in Table III. Low-energy cutoffs were chosen at a point where transmission falls below 1%. The thermal flux peaks at ≈0.08 eV and drops off rapidly with decreasing energy. The combination of low flux and the highly absorbing nature of gadolinium at subthermal energies led to regions of low transmission where the accuracy of the background treatment is important.

7. There were concerns about background in both epithermal transmission measurements using metal samples below 80 eV, and particularly below 10 eV. Therefore, the low-energy cutoff for these data sets was 10 eV.

The potential scattering lengths used in the present analysis for gadolinium are taken from ENDF. The potential scattering lengths used for deuterium and oxygen in the liquid samples were 5.20 and 5.46 fm, respectively. These radii were calculated from potential scattering cross sections, deuterium $\sigma_s = 3.4$ b and oxygen $\sigma_s = 3.75$ b (Ref. 27).

The potential scattering lengths for each of the gadolinium isotopes except ^{152}Gd were varied with SAMMY to obtain a better fit to the thick (5.08-mm) transmission data. The resulting potential scattering lengths were similar to ENDF, ±0.1 fm.

The radius to be used for penetrabilities and shifts were calculated using Eq. (3) (Ref. 8):

$$a = 1.23 \times AWRI^{1/3} + 0.8 \ , \qquad (3)$$

where a is the channel radius and *AWRI* is the atomic weight given in the ENDF file. This atomic weight is based on the mass of the neutron rather than amu.

The effective temperature was 293 K, and no external R-function was employed. Distant resonances were represented by including all of the resonances present in the ENDF file. No p-wave resonances were observed in the energy range currently being reported.

The manufacturer-specified tantalum content of the natural metal samples was 0.1%. A SAMMY fit of thick samples to the strong 4.28-eV resonance in tantalum yielded an abundance of 0.13%, which was used in all resonance parameter fits. That is, all ENDF resonances for Ta were included in all metal-sample SAMMY calculations with an abundance of 0.13%.

Resonance integrals are defined in Eq. (4):

$$RI = \int_{0.5eV}^{\infty} \sigma_C(E) \frac{dE}{E} \ , \qquad (4)$$

where *RI* is the infinitely dilute capture resonance integral (in barns) and $\sigma_C(E)$ is the neutron capture cross section (in barns).

Resonance integrals and thermal cross sections were calculated using the NJOY program.[28] The resonance integrals were evaluated from 0.5 eV to 20 MeV. One calculation was performed using ENDF resonance parameters, and one calculation was performed with RPI resonance parameters replacing the ENDF parameters for all resonances below 300 eV. Results are presented in Sec. VI.C.

VI. RESULTS

VI.A. Results: Thermal

Resonance parameters were determined in a covariance-matrix–linked SAMMY calculation. The resulting resonance parameters for the two thermal region resonances are given in Table IV. ENDF/B-VI resonance parameters are nearly identical to those of Møller et al.[3] The uncertainties given in Ref. 3 are reported as ENDF uncertainties in Table IV. The uncertainties given in Table IV for the thermal region were estimated to be on the order of 1σ and include the following considerations: internal consistency of the transmission data, reproducibility of transmission results, the uncertainty in capture flux normalization, and the balance of interactions between the overlapping ^{155}Gd and ^{157}Gd thermal resonances.

The methods used to estimate the RPI uncertainties are discussed in Sec. VII and Ref. 1. Since both of these

TABLE IV

Thermal Results: Resonance Parameters

Dataset	Energy (eV)	Γ_γ (meV)	Γ_n (meV)	Isotope	J
ENDF-B/VI	0.0268 ± 0.0002	108 ± 1	0.104 ± 0.002	155	2
	0.0314 ± 0.0002	106 ± 1	0.4704 ± 0.0080	157	2
RPI	0.025 ± 0.003	104 ± 3	0.097 ± 0.003	155	2
	0.032 ± 0.003	107 ± 3	0.428 ± 0.004	157	2

resonances are predominantly capture resonances, both transmission and capture measurements were essentially measuring capture. Neutron width is the resonance parameter that was most sensitive to the data in both capture and transmission. The neutron widths for both resonances were found to be smaller than ENDF, by 9% in the ^{157}Gd resonance and by 7% in the smaller ^{155}Gd resonance.

Fourteen samples were included in this calculation: seven liquid transmission samples (four enriched in ^{155}Gd, and three enriched in ^{157}Gd), three natural metal transmission samples, and four liquid capture samples (two enriched in ^{155}Gd and two enriched in ^{157}Gd). No natural metal capture measurements were made. An overview of the data and the SAMMY calculations using RPI resonance parameters is shown in Fig. 2. Comparisons of some of the present results to ENDF are shown in Fig. 3. The inability of a single set of resonance parameters to fit all data sets simultaneously is due to internal inconsistencies in the data. The SAMMY fit was a statistically weighted combination of the data sets. The name of each sample and the isotope in which it is enriched is given in the legends of Figs. 2 and 3. The isotopic content in each sample is given in Table II. The thermal-region ^{157}Gd resonance is approximately four times stronger than the ^{155}Gd resonance, and their relative abundances in natural metal are approximately the same (see Table II).

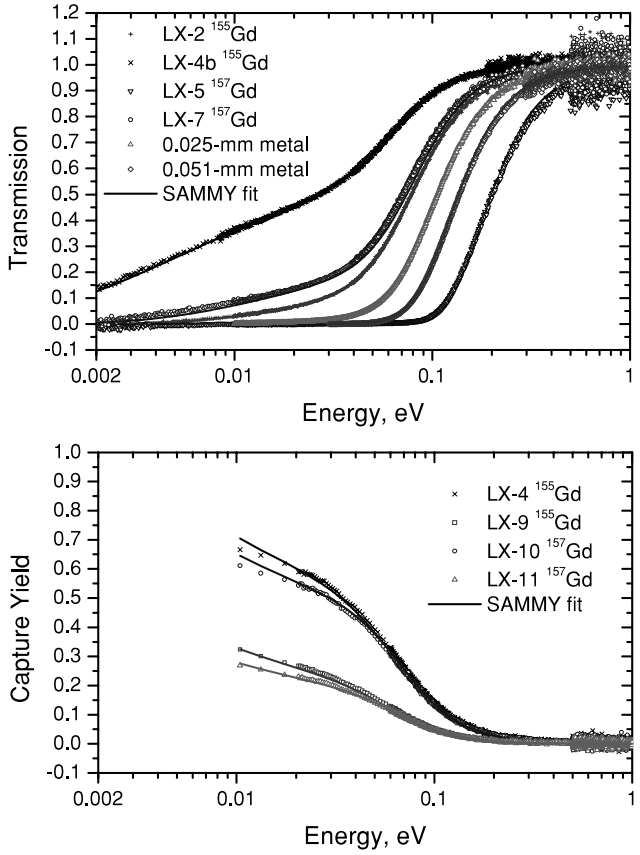

Fig. 2. An overview of transmission and capture data used in the thermal region and the SAMMY fits. The covariance matrix-linked fit represents the calculated transmissions and yields using RPI resonance parameters. Sample details are given in Tables II and III. "LX-4b" signifies data from sample LX-4 taken during the second thermal transmission experiment. Experimental details are given in Table I.

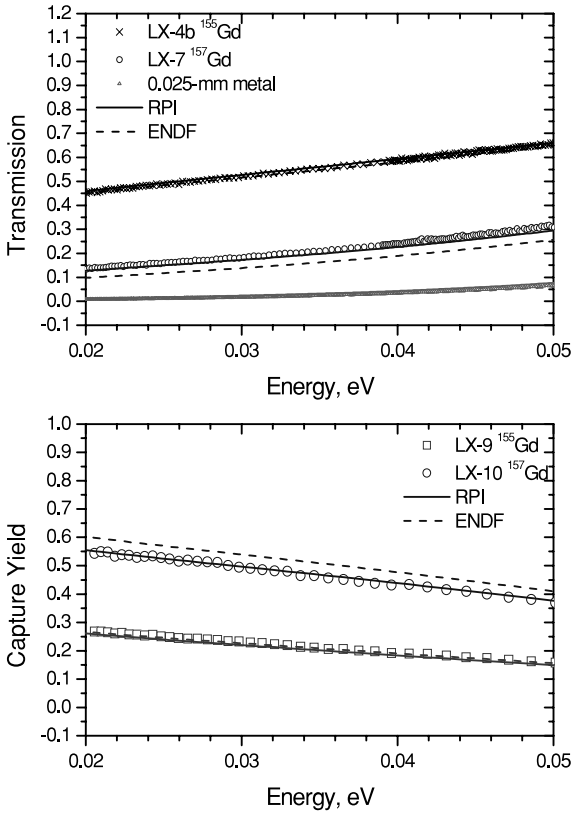

Fig. 3. The data for five thermal region samples, SAMMY fit and corresponding calculated transmissions and yields using ENDF resonance parameters. The thermal (0.0253-eV) capture cross section of ^{157}Gd was measured to be 9% lower than that of ENDF. The ^{155}Gd thermal capture cross section was not significantly different from ENDF. Sample details are given in Tables II and III. "LX-4b" signifies data from sample LX-4 taken during the second thermal transmission experiment. Experimental details are given in Table I.

The ^{157}Gd neutron width is determined predominantly from natural metal transmission data and ^{157}Gd-enriched liquid sample transmission data. Capture normalization, in turn, is determined predominantly by the transmission-derived ^{157}Gd neutron width. The ^{155}Gd neutron width is determined predominantly by ^{155}Gd-enriched liquid transmission data and, to a lesser extent, by natural metal transmission data and ^{155}Gd-enriched liquid sample capture data. In the present data, transmission data have smaller statistical uncertainties than capture yield data, and thick samples have more influence

on derived resonance parameters than thin samples in both capture and transmission.[21]

VI.B. Results: Epithermal

An overview of the SAMMY fit in the epithermal region is given in Fig. 4. The epithermal region was analyzed in two parts. First, the 1- to 10-eV region was fitted with a combination of thermal transmission and epithermal capture data sets (see Sec. V). Second, the 10- to 300-eV region was fitted using data entirely from natural metal samples in capture and transmission. Resonance parameters for the epithermal region are given in Table V. The uncertainties quoted in Table V for the epithermal region were estimated to be on the order of 1σ, are described in Sec. VII and Ref. 1, and include the following considerations: consistency between capture and transmission results, stability of radiation widths, uncertainty in transmission background treatment, and Bayesian statistical errors. There are 28 new resonances introduced that were not included in ENDF. Six resonances present in ENDF have been discarded because the literature does not demonstrate their existence nor do the present measurements support their existence. Parameters for several resonances, particularly those from ^{152}Gd, were not fitted because the resonances were very weak. In these cases the resonance parameters are assigned ENDF values and are listed in Table V without any quoted errors.

VI.B.1. Results: Epithermal—The 1- to 10-eV Region

Resonance parameters resulting from the SAMMY fit are given in Table V. The same three samples were measured in both transmission and capture, i.e., 0.025 mm (1 mil), 0.051 mm (2 mil), and 0.127 mm (5 mil) natural metal Gd. The radiation width for the weak 3.6-eV resonance in ^{155}Gd was not varied from ENDF values.

VI.B.2. Results: Epithermal—The 10- to 300-eV Region

Fifteen data sets were used in the region above 10 eV. There were two separate transmission measurements. The first used a B_4C overlap filter and included samples of the following thicknesses: 0.127 mm (5 mil), 0.254 mm (10 mil), 0.508 mm (20 mil), 0.889 mm (35 mil), and 1.27 mm (50 mil). The second epithermal transmission measurement used a Cd overlap filter and included samples of the following thicknesses: 0.508 mm (20 mil), 0.889 mm (35 mil), 1.27 mm (50 mil), 2.54 mm (100 mil), 5.08 mm (200 mil), and 1.02 cm (400 mil). The capture measurement used a Cd overlap filter and included samples of the following thicknesses: 0.025 mm (1 mil), 0.051 mm (2 mil), 0.127 mm (5 mil), and 2.54 mm (100 mil).

The resolved resonance energy region for ^{155}Gd in the ENDF/B-VI evaluation ends at 180 eV. As a result,

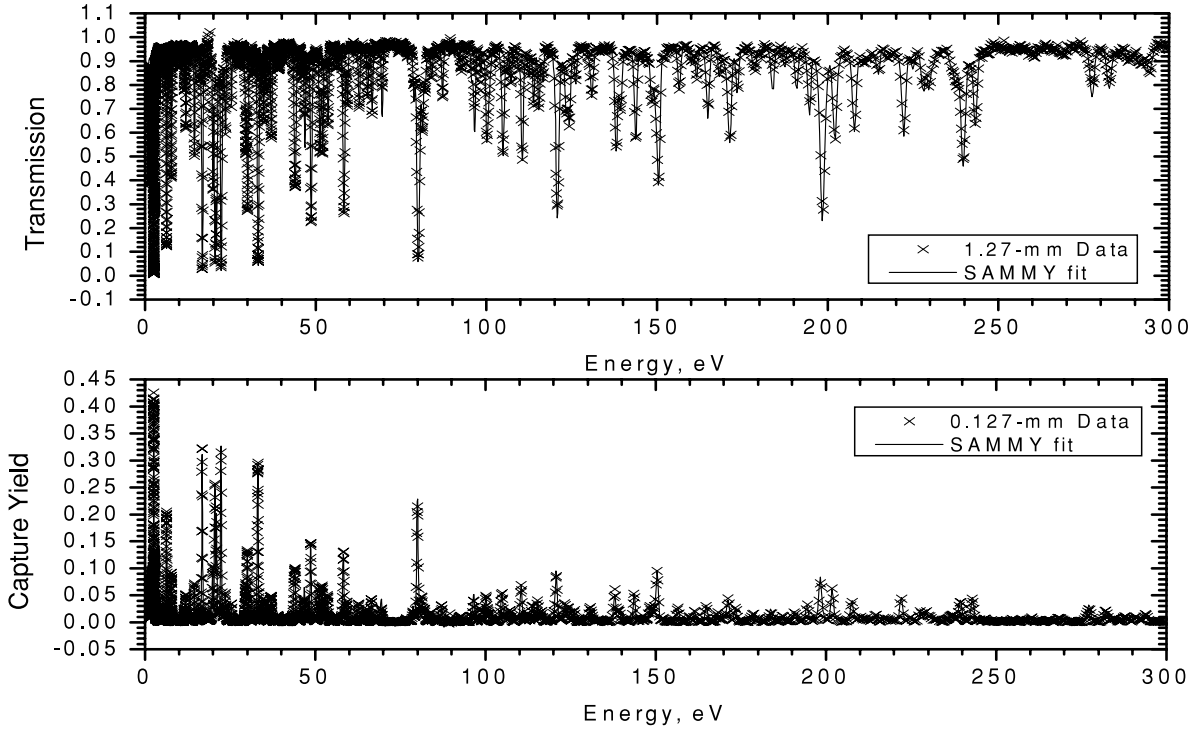

Fig. 4. An overview of the data and SAMMY fits in the epithermal region.

TABLE V

Epithermal Results: Resonance Parameters

Energy (eV)	Energy ENDF (meV)	Γ_γ (meV)	Γ_γ ENDF (meV)	Γ_n ($2ag\Gamma_n$ for unassigned) (meV)	Γ_n ENDF (meV)	Isotope ENDF	J ENDF
2.0120 ± 0.0002	2.008	128 ± 1	110.00	0.40 ± 0.01	0.371	155	1
2.5729 ± 0.0003	2.568	107.1 ± 0.4	111.00	1.706 ± 0.003	1.744	155	2
2.8287 ± 0.0003	2.825	109.7 ± 0.9	97.00	0.377 ± 0.004	0.345	157	2
3.616 ± 0.003	3.616	130	130.00	0.05 ± 0.02	0.044	155	1
6.3057 ± 0.0002	6.300	108.8 ± 0.6	114.00	2.20 ± 0.01	2.000	155	2
7.7477 ± 0.0004	7.750	109 ± 1	124.00	1.16 ± 0.01	1.120	155	2
9.991 ± 0.003	10.010	110 ± 20	115.00	0.20 ± 0.04	0.168	155	2
11.508 ± 0.001	11.530	120 ± 40	125.00	0.78 ± 0.08	0.600	155	1
11.57 ± 0.05	11.580	90 ± 80	88.00	0.2 ± 0.2	0.350	154	$\frac{1}{2}$
11.964 ± 0.008	11.990	130 ± 20	112.00	1.12 ± 0.04	0.880	155	2
12.35	12.350	58.6	58.60	4.65	4.650	152	$\frac{1}{2}$
14.476 ± 0.009	14.510	130 ± 10	103.00	3.43 ± 0.09	3.200	155	1
16.201 ± 0.005	16.240	130 ± 30	91.00	0.44 ± 0.03	0.400	157	1
16.78 ± 0.01	16.770	112 ± 7	80.50	13.9 ± 0.5	12.800	157	2
17.729 ± 0.005	17.770	130 ± 40	120.00	0.47 ± 0.04	0.392	155	2
19.86 ± 0.01	19.920	118 ± 6	104.00	4.5 ± 0.1	4.560	155	2
20.51 ± 0.02	20.560	106 ± 8	88.00	13.4 ± 0.4	11.360	157	2
20.97 ± 0.02	21.030	140 ± 20	98.00	11.6 ± 0.5	15.600	155	2
21.59 ± 0.02	21.650	80 ± 40	114.00	0.34 ± 0.08	0.376	157	2
22.30 ± 0.04	22.300	100 ± 40	96.00	7.1 ± 0.8	6.000	158	$\frac{1}{2}$
22.5 ± 0.2	22.330	100 ± 100	88.00	20 ± 10	11.500	154	$\frac{1}{2}$
23.28 ± 0.03	23.330	140 ± 30	121.00	1.3 ± 0.3	0.813	157	1
23.60 ± 0.02	23.670	140 ± 10	120.00	2.91 ± 0.08	3.120	155	2
25.35 ± 0.01	25.400	130 ± 30	85.00	1.99 ± 0.06	1.840	157	2
27.509 ± 0.002	27.570	140 ± 20	125.00	1.31 ± 0.04	1.120	155	1
29.50 ± 0.02	29.580	113 ± 2	108.00	4.8 ± 0.1	4.320	155	2
30.05 ± 0.02	30.100	130 ± 10	100.00	11.1 ± 0.5	10.400	155	2
31.66 ± 0.01	31.720	140 ± 20	118.00	1.24 ± 0.07	1.120	155	2
33.1 ± 0.2	33.140	110 ± 30	109.80	1.6 ± 0.6	1.867	155	1
33.14 ± 0.03	33.230	98 ± 3	90.00	14 ± 2	14.600	156	$\frac{1}{2}$
33.4 ± 0.3	33.510	120 ± 90	115.00	1 ± 4	1.600	155	1
34.73 ± 0.02	34.830	131 ± 4	152.00	6.8 ± 0.2	6.133	155	1
35.39 ± 0.01	35.470	140 ± 10	118.00	2.17 ± 0.06	1.840	155	2
36.86	36.860	56	56.00	84	84.000	152	$\frac{1}{2}$
37.066 ± 0.003	37.120	139 ± 6	101.00	8.3 ± 0.3	8.400	155	1
38.93 ± 0.01	39.000	130 ± 60	118.00	1.25 ± 0.07	1.040	155	2
39.30	39.300	56	56.00	39	39.000	152	$\frac{1}{2}$
40.08 ± 0.01	40.170	120 ± 40	110.00	1.6 ± 0.2	1.307	157	1
42.73	42.730	56	56.00	3.06	3.060	152	$\frac{1}{2}$
43.83 ± 0.07	43.920	140 ± 90	136.00	18 ± 9	17.333	155	1
44.11 ± 0.04	44.220	120 ± 70	96.00	9 ± 5	8.960	157	2
45.98 ± 0.02	46.100	128 ± 6	126.00	2.3 ± 0.1	2.240	155	2
46.79 ± 0.02	46.870	140 ± 30	100.00	10.2 ± 0.4	5.360	155	2
47.18 ± 0.04	47.070	89 ± 8	88.00	2.4 ± 0.6	3.200	154	$\frac{1}{2}$
47.628 ± 0.006	47.730	107 ± 10	109.80	0.39 ± 0.03	0.653	155	1
48.68 ± 0.03	48.790	118 ± 9	90.00	26.7 ± 0.5	24.000	157	2
49.63 ± 0.07	49.500	90 ± 40	88.00	3 ± 1	1.800	154	$\frac{1}{2}$
51.25 ± 0.03	51.380	130 ± 30	109.80	20.3 ± 0.6	18.667	155	1
52.01 ± 0.03	52.130	140 ± 20	115.00	20.9 ± 0.8	19.467	155	1
52.89 ± 0.02	53.030	80 ± 30	109.80	1.2 ± 0.2	1.360	155	2
53.62 ± 0.02	53.740	140 ± 30	92.00	8.7 ± 0.2	7.680	155	2
56.12 ± 0.01	56.220	120 ± 40	120.00	2.5 ± 0.1	2.160	155	2
58.26 ± 0.03	58.300	140 ± 20	101.00	32.0 ± 0.6	28.000	157	2

(Continued)

TABLE V (Continued)

Energy (eV)	Energy ENDF (meV)	Γ_γ (meV)	Γ_γ ENDF (meV)	Γ_n ($2ag\Gamma_n$ for unassigned) (meV)	Γ_n ENDF (meV)	Isotope ENDF	J ENDF
59.30 ± 0.01	59.320	140 ± 40	129.00	6.9 ± 0.4	6.640	155	2
62.73 ± 0.02	62.840	150 ± 30	90.00	8.5 ± 0.5	8.000	155	2
64.028 ± 0.006	64.090	110 ± 40	109.80	0.49 ± 0.05	0.256	155	2
65.21 ± 0.01	65.060	100 ± 20	57.00	32 ± 5	24.000	154	$\frac{1}{2}$
66.4 ± 0.5	65.200	120 ± 10	109.80	0.5 ± 0.4	1.333	155	1
66.53 ± 0.01	66.560	130 ± 60	67.00	16 ± 2	14.667	157	1
69.4 ± 0.1	69.400	100 ± 100	109.80	12 ± 4	6.320	155	2
74.34	74.340	50.4	50.40	60	60.000	152	$\frac{1}{2}$
76.00 ± 0.03	76.120	90 ± 50	88.00	2.0 ± 0.9	1.100	154	$\frac{1}{2}$
76.85 ± 0.01	77.000	110 ± 60	109.80	3.0 ± 0.3	1.600	155	2
77.63 ± 0.01	77.800	110 ± 20	109.80	0.9 ± 0.1	1.200	155	1
78.75 ± 0.06	78.800	110 ± 30	109.80	8 ± 1	4.240	155	2
80.04 ± 0.07	80.200	80 ± 7	86.00	80 ± 20	50.900	156	$\frac{1}{2}$
80 ± 1	80.050	112 ± 4	109.80	0 ± 3	0.312	155	2
80.9 ± 0.3	80.900	110 ± 30	109.80	1.44 ± 0.09	2.400	155	1
81.30 ± 0.04	81.480	110 ± 40	108.00	24 ± 2	20.000	157	1
82.10 ± 0.04	82.240	100 ± 70	99.95	7.1 ± 0.6	6.160	157	2
83.97 ± 0.02	84.200	120 ± 40	109.80	10.3 ± 0.1	9.200	155	1
84.91 ± 0.01	85.000	110 ± 40	109.80	2.2 ± 0.3	3.067	155	1
85.55	85.550	58.6	58.60	5.11	5.110	152	$\frac{1}{2}$
87.17 ± 0.03	87.210	140 ± 10	128.00	11.1 ± 0.4	10.160	157	2
90.51 ± 0.02	90.500	110 ± 90	109.80	2.5 ± 0.2	1.280	155	2
92.40	92.400	58.6	58.60	142	142.000	152	$\frac{1}{2}$
92.47 ± 0.02	92.500	110 ± 20	109.80	2.14 ± 0.06	2.160	155	2
92.90 ± 0.03	92.800	110 ± 50	109.80	3.48 ± 0.07	3.120	155	2
93.99 ± 0.01	94.100	110 ± 40	109.80	0.64 ± 0.09	0.544	155	2
95.70 ± 0.03	95.700	110 ± 50	109.80	7.1 ± 0.4	3.840	155	2
96.4 ± 0.2	96.600	110 ± 50	109.80	3.8 ± 0.7	6.267	155	1
96.6 ± 0.1	96.520	100 ± 40	110.00	22.0 ± 0.4	12.160	157	2
98.30 ± 0.03	98.300	150 ± 20	109.80	11.7 ± 0.4	17.333	155	1
99.9 ± 0.1	100.200	110 ± 10	109.80	2.5 ± 0.2	2.133	155	1
100.16 ± 0.06	100.200	100 ± 30	94.00	43 ± 1	46.667	157	1
100.72 ± 0.08	100.700	90 ± 40	82.00	48 ± 7	32.000	154	$\frac{1}{2}$
101.20 ± 0.09	101.100	120 ± 10	105.00	1.3 ± 0.2	1.000	158	$\frac{1}{2}$
101.42 ± 0.02	101.400	140 ± 30	109.80	2.1 ± 0.2	2.720	155	2
102.03 ± 0.03	102.100	110 ± 50	109.80	1.52 ± 0.06	1.733	155	1
104.36 ± 0.09	104.400	110 ± 80	109.80	5 ± 1	9.067	155	1
104.89 ± 0.08	104.950	103 ± 2	70.00	70 ± 40	57.333	157	1
105.8 ± 0.1	105.900	140 ± 20	109.80	6 ± 1	6.133	155	1
106.05 ± 0.08	105.600	110 ± 20	88.00	11 ± 2	4.800	154	$\frac{1}{2}$
107.14 ± 0.04	107.100	110 ± 80	109.80	9 ± 2	6.240	155	2
107.46 ± 0.06	107.460	120 ± 30	99.95	4 ± 1	5.600	157	2
109.37 ± 0.02	109.600	115 ± 2	109.80	7.3 ± 0.5	4.667	155	1
110.54 ± 0.07	110.460	140 ± 50	85.00	50 ± 20	42.400	157	2
112.40 ± 0.04	112.400	90 ± 70	84.00	9.1 ± 0.2	9.040	155	2
113.81 ± 0.05	113.800	130 ± 20	67.00	20 ± 1	15.200	155	2
115.37 ± 0.06	115.350	140 ± 20	112.00	22.2 ± 0.9	19.200	157	2
116.56 ± 0.06	116.500	120 ± 80	116.00	21 ± 1	17.333	155	1
118.66 ± 0.02	118.600	110 ± 50	109.80	2.5 ± 0.4	2.000	155	2
120.83 ± 0.01	121.000	130 ± 30	91.00	140 ± 40	132.000	157	2
123.35 ± 0.05	123.400	200 ± 100	159.00	40 ± 6	36.000	155	1
124.25 ± 0.08	124.000	110 ± 50	85.00	150 ± 20	124.000	154	$\frac{1}{2}$
124.49 ± 0.03	124.400	120 ± 20	109.80	4 ± 1	6.640	155	2
126.11 ± 0.02	126.000	110 ± 60	109.80	14.6 ± 0.4	20.533	155	1

(Continued)

TABLE V (Continued)

Energy (eV)	Energy ENDF (meV)	Γ_γ (meV)	Γ_γ ENDF (meV)	Γ_n ($2ag\Gamma_n$ for unassigned) (meV)	Γ_n ENDF (meV)	Isotope ENDF	J ENDF
128.53 ± 0.02	128.600	110 ± 30	109.80	1.7 ± 0.2	1.120	155	2
129.82 ± 0.01	129.800	110 ± 40	109.80	3.4 ± 0.3	2.560	155	2
130.79 ± 0.01	130.800	150 ± 30	109.80	22 ± 3	48.533	155	1
131.37 ± 0.01	New	130 ± 10	New	1.27 ± 0.08	New	Unassigned	
133.04 ± 0.01	133.000	140 ± 20	109.80	5.3 ± 0.4	3.733	155	1
133.95 ± 0.01	133.800	110 ± 30	109.80	3.4 ± 0.2	2.320	155	2
135.13 ± 0.02	134.700	110 ± 60	109.80	1.9 ± 0.1	0.880	155	2
Discarded	135.100		99.95		0.880	157	2
Discarded	137.900		99.95		78.667	157	1
137.99 ± 0.08	137.800	120 ± 80	109.80	90 ± 30	21.333	155	1
138.2 ± 0.2	138.700	100 ± 10	86.00	21 ± 9	82.667	157	1
138.9 ± 0.2	139.200	94 ± 8	91.00	40 ± 10	124.000	154	$\frac{1}{2}$
139.37 ± 0.05	139.300	100 ± 70	99.95	40 ± 10	10.000	157	1
140.00	140.000	58.6	58.60	78.8	78.800	152	$\frac{1}{2}$
140.55 ± 0.05	140.400	130 ± 10	109.80	4.9 ± 0.3	4.133	155	1
141.30 ± 0.01	141.400	120 ± 10	109.80	1.69 ± 0.08	1.040	155	2
143.75 ± 0.01	143.610	130 ± 30	88.00	60 ± 10	60.000	157	2
145.66 ± 0.01	145.600	150 ± 20	109.80	6.5 ± 0.3	6.160	155	2
147.02 ± 0.01	146.900	130 ± 10	109.80	5.3 ± 0.2	3.760	155	2
148.2 ± 0.2	148.400	120 ± 20	88.00	46 ± 10	38.000	154	$\frac{1}{2}$
148.4 ± 0.3	148.200	110 ± 10	109.80	8.6 ± 0.9	9.600	155	2
148.55 ± 0.05	148.310	140 ± 30	99.95	24 ± 1	24.000	157	1
149.53 ± 0.03	149.600	110 ± 40	109.80	36 ± 2	33.333	155	1
150.37 ± 0.04	150.200	110 ± 40	109.80	80 ± 30	24.800	155	2
150.62 ± 0.03	151.200	80 ± 30	86.00	23 ± 7	41.700	156	$\frac{1}{2}$
152.27 ± 0.01	152.200	150 ± 40	109.80	6.2 ± 0.8	8.000	155	1
153.80 ± 0.05	154.000	160 ± 30	109.80	1.1 ± 0.2	1.120	155	2
156.4 ± 0.1	156.300	110 ± 80	109.80	30 ± 10	7.680	155	2
156.70 ± 0.02	156.430	140 ± 50	91.00	13 ± 5	19.760	157	2
160.00	160.000	58.6	58.60	2.83	2.830	152	$\frac{1}{2}$
160.03 ± 0.07	160.100	110 ± 50	109.80	10.3 ± 0.5	9.600	155	2
161.57 ± 0.08	161.600	150 ± 20	109.80	21.6 ± 0.8	20.000	155	2
164.8 ± 0.2	164.500	98 ± 7	77.00	158 ± 2	105.000	154	$\frac{1}{2}$
165.00 ± 0.09	164.830	100 ± 80	100.00	23 ± 6	20.560	157	2
168.20 ± 0.09	168.300	123 ± 6	109.80	31 ± 4	30.133	155	1
168.60 ± 0.04	168.030	99.95	99.95	3.333	3.333	157	1
169.4 ± 0.1	169.250	90 ± 10	99.95	3.4 ± 0.2	3.280	157	2
170.2 ± 0.1	170.300	80 ± 30	109.80	8 ± 1	8.320	155	2
170.4 ± 0.1	170.400	85 ± 9	88.00	4.9 ± 0.4	5.000	154	$\frac{1}{2}$
171.2 ± 0.2	171.250	100 ± 10	99.95	120 ± 40	44.000	157	1
171.6 ± 0.1	171.400	110 ± 60	109.80	18 ± 1	9.200	155	2
173.5 ± 0.1	173.500	110 ± 80	109.80	33 ± 2	32.800	155	2
173.80	173.800	30.1	30.10	86	86.000	152	$\frac{1}{2}$
175.46 ± 0.05	175.600	110 ± 40	109.80	4.2 ± 0.6	2.080	155	2
177.99 ± 0.02	178.000	130 ± 10	109.80	13 ± 2	9.733	155	1
178.73 ± 0.03	178.550	140 ± 20	145.00	17.0 ± 1.0	16.000	157	2
180.34 ± 0.04	180.400	110 ± 40	109.80	9.7 ± 0.3	14.667	155	1
183.20 ± 0.05	New	110 ± 40	New	1.3 ± 0.2	New	Unassigned	
183.94 ± 0.07	183.830	100 ± 90	99.95	34 ± 8	17.600	157	2
185.11 ± 0.04	New	110 ± 60	New	0.6 ± 0.1	New	Unassigned	
185.70	185.700	52.5	52.50	84	84.000	152	$\frac{1}{2}$
187.36 ± 0.07	New	100 ± 100	New	3.5 ± 0.2	New	Unassigned	
189.30 ± 0.06	New	100 ± 80	New	0.3 ± 0.1	New	Unassigned	
190.9 ± 0.1	190.730	100 ± 90	99.95	60 ± 60	28.000	157	1

(Continued)

TABLE V (Continued)

Energy (eV)	Energy ENDF (meV)	Γ_γ (meV)	Γ_γ ENDF (meV)	Γ_n ($2ag\Gamma_n$ for unassigned) (meV)	Γ_n ENDF (meV)	Isotope ENDF	J ENDF
194.6 ± 0.1	194.530	110 ± 50	99.95	60 ± 80	44.800	157	2
198.4 ± 0.2	198.100	92 ± 4	86.00	200 ± 100	270.000	156	$\frac{1}{2}$
199.5 ± 0.2	201.600	60 ± 40	88.00	80 ± 50	11.700	154	$\frac{1}{2}$
Discarded	201.600		86.00		17.000	156	$\frac{1}{2}$
201.99 ± 0.01	202.100	160 ± 40	86.00	50 ± 10	266.000	156	$\frac{1}{2}$
Discarded	202.740		99.95		9.600	157	1
203.10	203.100	58.8	58.80	97	97.000	152	$\frac{1}{2}$
203.39 ± 0.02	New	130 ± 10	New	0.98 ± 0.04	New	Unassigned	
205.75 ± 0.04	205.350	110 ± 10	99.95	2.0 ± 0.1	0.976	157	2
Discarded	206.900		99.95		1.360	157	2
Discarded	207.700		58.60		5.230	152	$\frac{1}{2}$
207.77 ± 0.04	207.810	150 ± 20	114.00	110 ± 30	108.000	157	2
209.1 ± 0.2	New	120 ± 10	New	1.1 ± 0.2	New	Unassigned	
210.32 ± 0.01	New	140 ± 20	New	2.78 ± 0.06	New	Unassigned	
211.57 ± 0.02	211.000	99 ± 8	88.00	45 ± 1	35.000	154	$\frac{1}{2}$
212.32 ± 0.02	New	100 ± 10	New	0.64 ± 0.02	New	Unassigned	
213.68 ± 0.02	New	102 ± 10	New	1.02 ± 0.03	New	Unassigned	
214.77 ± 0.01	New	130 ± 20	New	5.5 ± 0.5	New	Unassigned	
217.23 ± 0.01	217.150	121 ± 9	99.95	19.9 ± 0.9	8.000	157	1
218.57 ± 0.02	New	140 ± 10	New	1.89 ± 0.03	New	Unassigned	
220.24 ± 0.08	220.900	150 ± 20	99.95	8.3 ± 0.4	4.000	157	1
222.22 ± 0.03	222.000	80 ± 20	120.00	50 ± 20	50.000	160	$\frac{1}{2}$
223.30	223.300	64.2	64.20	301	301.000	152	$\frac{1}{2}$
224.90 ± 0.02	224.000	100 ± 100	88.00	110 ± 60	18.000	154	$\frac{1}{2}$
227.91 ± 0.02	228.300	100 ± 100	99.95	52 ± 3	6.560	157	2
229.52 ± 0.02	New	100 ± 70	New	9.7 ± 0.5	New	Unassigned	
230.86 ± 0.05	New	100 ± 100	New	3.7 ± 0.2	New	Unassigned	
231.40	231.400	62	62.00	46	46.000	152	$\frac{1}{2}$
232.85 ± 0.01	New	100 ± 90	New	2.2 ± 0.2	New	Unassigned	
235.9 ± 0.2	New	70 ± 60	New	1.4 ± 0.2	New	Unassigned	
237.3 ± 0.1	New	100 ± 100	New	5.8 ± 0.2	New	Unassigned	
238.00	238.000	100	100.00	223.6	223.600	152	$\frac{1}{2}$
239.56 ± 0.03	239.550	120 ± 20	99.95	250 ± 40	152.000	157	2
243.17 ± 0.01	242.700	90 ± 20	105.00	50 ± 20	60.000	158	$\frac{1}{2}$
245.16 ± 0.02	244.000	98 ± 9	86.00	3.25 ± 0.06	3.100	156	$\frac{1}{2}$
246.80 ± 0.01	244.600	118 ± 9	99.95	19.8 ± 0.5	4.400	157	1
248.83 ± 0.01	246.640	120 ± 10	99.95	5.0 ± 0.1	9.280	157	2
250.51 ± 0.02	250.200	130 ± 10	99.95	8.2 ± 0.2	5.733	157	1
252.40	252.400	52.4	52.40	127	127.000	152	$\frac{1}{2}$
253.25 ± 0.03	252.800	101 ± 9	88.00	26 ± 1	12.000	154	$\frac{1}{2}$
254.87 ± 0.01	255.000	130 ± 10	99.95	18.6 ± 0.5	3.600	157	1
256.46 ± 0.06	255.200	101 ± 10	99.95	1.46 ± 0.09	3.733	157	1
258.01 ± 0.01	257.500	91 ± 7	88.00	40 ± 1	34.000	154	$\frac{1}{2}$
259.25 ± 0.02	New	102 ± 10	New	1.11 ± 0.03	New	Unassigned	
260.53 ± 0.01	260.500	120 ± 10	99.95	31 ± 3	21.867	157	1
262.56 ± 0.01	New	104 ± 10	New	0.96 ± 0.02	New	Unassigned	
264.89 ± 0.01	New	110 ± 10	New	1.30 ± 0.03	New	Unassigned	
266.05 ± 0.01	265.610	110 ± 10	99.95	7.9 ± 0.2	6.400	157	2
268.47 ± 0.01	268.020	140 ± 20	99.95	17.0 ± 0.9	10.480	157	2
269.57 ± 0.03	269.200	120 ± 20	88.00	50 ± 10	28.000	154	$\frac{1}{2}$
272.36 ± 0.02	New	100 ± 60	New	1.3 ± 0.1	New	Unassigned	
277.38 ± 0.06	277.200	100 ± 300	105.00	40 ± 60	18.000	158	$\frac{1}{2}$
279.40 ± 0.03	New	98 ± 10	New	0.44 ± 0.03	New	Unassigned	
282.60	282.600	49.1	49.10	145	145.000	152	$\frac{1}{2}$

(Continued)

TABLE V (Continued)

Energy (eV)	Energy ENDF (meV)	Γ_γ (meV)	Γ_γ ENDF (meV)	Γ_n ($2ag\Gamma_n$ for unassigned) (meV)	Γ_n ENDF (meV)	Isotope ENDF	J ENDF
282.28 ± 0.05	281.640	110 ± 100	99.95	70 ± 30	38.400	157	2
284.2 ± 0.1	New	100 ± 30	New	2.1 ± 0.2	New	Unassigned	
285.24 ± 0.05	New	150 ± 40	New	2.7 ± 0.4	New	Unassigned	
287.89 ± 0.04	287.330	100 ± 50	99.95	25 ± 3	14.240	157	2
288.99 ± 0.03	New	140 ± 30	New	2.3 ± 0.3	New	Unassigned	
291.08 ± 0.03	290.770	100 ± 50	99.95	51 ± 9	65.333	157	1
292.37 ± 0.07	New	130 ± 30	New	2.2 ± 0.2	New	Unassigned	
293.40	293.400	71	71.00	352	352.000	152	$\frac{1}{2}$
294.16 ± 0.01	293.700	130 ± 30	99.95	49 ± 8	36.800	157	2
295.79 ± 0.08	New	100 ± 10	New	0.5 ± 0.2	New	Unassigned	
298.0 ± 0.1	New	110 ± 10	New	0.38 ± 0.08	New	Unassigned	

fitting data above 180 eV was performed without initial estimates for resonance locations and widths—a challenging task.

Finally, if a resonance is clearly observed in both transmission and capture, it has been added to the database shown in Table V. In these cases, the isotope and spin are listed as unassigned, and their associated neutron widths are given as $2ag\Gamma_n$, where a is abundance and g is the statistical weighting factor: $g = (2J + 1)/[2(2I + 1)]$, where I is the spin of the target nucleus and J is the total angular momentum of the compound state (also known as the spin state of the resonance) in units of $h/2\pi$ where h is Planck's constant.

An example of the detailed descriptions available for the entire epithermal region in Ref. 1 is repeated here for the 200- to 225-eV region. Resonances in this region are shown in Fig. 5. Four resonances from ENDF have been excluded from the present analysis: 201.6 eV in

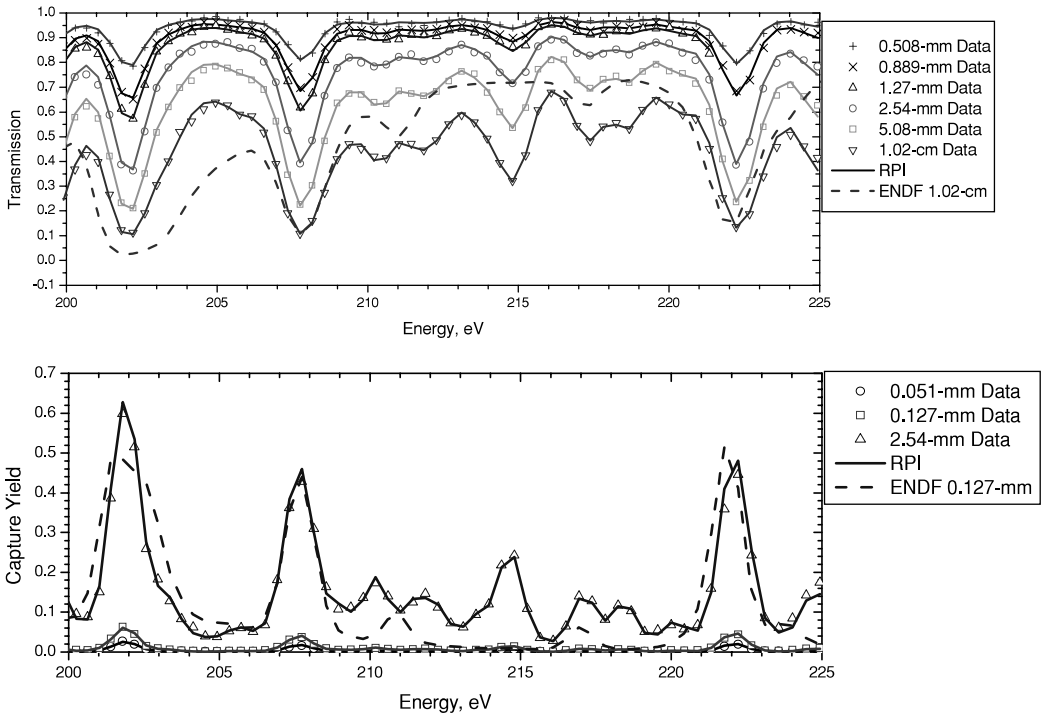

Fig. 5. An overview of transmission and capture data used in the 200- to 225-eV region and the SAMMY fits using the RPI parameters. The dashed lines represent the ENDF parameters for the thickest samples.

^{156}Gd, 202.74 eV in ^{157}Gd, 206.9 eV in ^{157}Gd, and 207.7 eV in ^{152}Gd. There are two reasons for these omissions. First, no author has explicitly seen any of these four resonances. Second, inclusion of these resonances does not improve the fit to the data.

There are four resonances listed in ENDF in the 201- to 203-eV region. The first of these, at 201.6 eV in ^{154}Gd, was identified by Ref. 7. It has been moved to 199.4 eV in the present fit. The next two resonances, 201.6 eV in ^{156}Gd and 202.1 eV in ^{156}Gd, have never both been observed. Mughabghab and Chrien[4] and Coceva and Stefanon[29] each saw a single resonance at 202.1 and 201.8 eV, respectively. However, two resonances are listed in Ref. 27 and in ENDF. Only one resonance is listed at 202 eV in ^{156}Gd in the present analysis. Another specific omission of a resonance listed in ENDF occurred at 206.9 eV in ^{157}Gd. This resonance is small in ENDF, $\Gamma_n = 1.36$ meV, and cannot be traced to any of the Gd experiments discussed in this paper. It does not improve the fit and has been omitted from the present results. ENDF contains a ^{152}Gd resonance at 207.7 eV, but a review of the literature failed to reveal the source of this resonance. While, in general, ^{152}Gd resonances were not varied, this particular resonance was omitted from the present analysis. The effect of removing this resonance on the widths of the nearest resonance at 207.8 eV is negligible.

Seven new resonances have been added in the 200- to 225-eV region. The first, at 203.1 eV, is a shoulder on the 202-eV resonance in ^{156}Gd (see Fig. 5). A new resonance has been proposed at 209.1 eV. It is a shoulder on the larger 207.77-eV resonance in ^{157}Gd. Five more resonances have been assigned at 210.32, 212.32, 213.68, 214.77, and 218.57 eV to account for structure apparent in the data in Fig. 5.

VI.B.3. Results: Epithermal—Justification for New Resonances

Figure 6 shows a "staircase" plot of gadolinium level density including all new resonances added during the present analysis. The plot of observed levels versus energy shows a good fit to a straight line that agrees with the statistical model of the nucleus up to ~50 eV. All levels are s-wave. Elemental gadolinium is shown because there is no assignment of isotope to the proposed new resonances. Above 50 eV a significant number of levels are missed. Therefore, even with the resonances added in the present analysis, the expectation of constant level density versus energy is not exceeded.

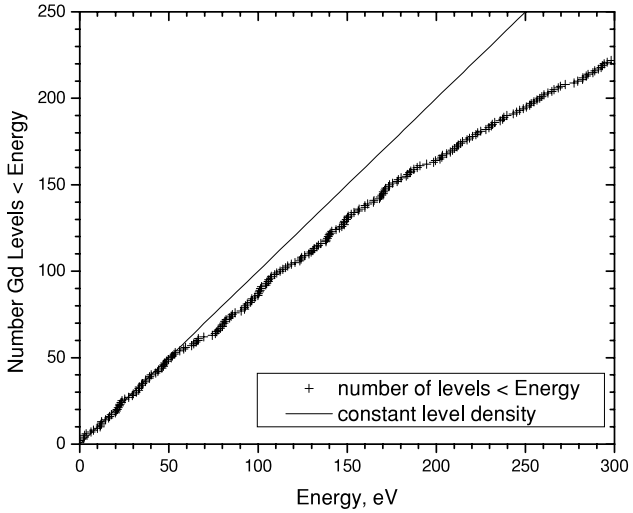

Fig. 6. Staircase plot of elemental gadolinium observed levels versus energy shows a good fit to a straight line up to ~50 eV. Above 50 eV, even with the resonances added in the present analysis, the expectation of constant level density versus energy is not exceeded.

VI.C. Results: Resonance Integrals and Thermal Cross Sections

Thermal cross sections and infinitely dilute capture resonance integrals have been calculated using ENDF and RPI resonance parameters. The isotopic ENDF evaluations used are from ENDF/B-VI updated through release 8. These files were processed using NJOY (Ref. 28) into pointwise (energy and cross-section) data, and isotopic thermal (2200 m/s) cross sections were obtained. The original ENDF files were then modified by replacing the original file 2 resonance parameters with those determined in the present work for all resonances below 300 eV. All resonances listed in Tables IV and V, except those designated "Unassigned" in those tables, were included. The resulting modified-ENDF files were processed using NJOY (Ref. 28), and thermal cross sections and resonance integrals were obtained.

Thermal cross sections from the present measurements are compared to those of ENDF in Tables VI and VII. The most significant departure of the present results from ENDF thermal capture cross sections is in ^{157}Gd. This 11% reduction (from 254 000 b for ENDF to 226 000 b for RPI) is consistent with the ≈9% reduction in neutron width for the thermal ^{157}Gd resonance (see Table IV). An insignificant reduction in thermal capture cross section is seen in ^{155}Gd. This is due to the competing effects of a 7% reduction in neutron width compensated by a 3.7% reduction in total width ($\Gamma_n + \Gamma_\gamma$) and an energy shift toward the thermal energy (0.0253 eV) point. The thermal capture cross section of elemental gadolinium is ≈9% lower than that calculated from ENDF parameters.

A significant reduction of the thermal elastic cross section (Table VII) of the present results from ENDF occurs in ^{157}Gd (from 1010 to 798 b). Thermal elastic scattering cross sections are proportional to Γ_n^2. So, the reduction in the thermal elastic cross section of ^{157}Gd is consistent with the ≈9% reduction in neutron width for

TABLE VI

Thermal Capture Cross Sections: A Comparison of ENDF/B-VI to RPI Results*

Thermal Capture Cross Sections							
		ENDF			RPI		
Isotope	Abundance	Thermal Capture	Contribution to Elemental	Percent	Thermal Capture	Contribution to Elemental	Percent
^{152}Gd	0.200	1 050	2.10	0.00430	1 050	2.10	0.00430
^{154}Gd	2.18	85.0	1.85	0.00379	85.8	1.87	0.00422
^{155}Gd	14.80	60 700	8 980	18.4	60 200	8 910	20.1
^{156}Gd	20.47	1.71	0.350	0.000717	1.74	0.356	0.000804
^{157}Gd	15.65	254 000	39 800	81.6	226 000	35 400	79.9
^{158}Gd	24.84	2.01	0.499	0.00102	2.19	0.544	0.00122
^{160}Gd	21.86	0.765	0.167	0.000342	0.755	0.165	0.000372
Gd	—		48 800	100.0		44 300	100.0

*The units of all cross sections are barns. The units of abundance are percent.

TABLE VII

Thermal Elastic Scattering Cross Sections: A Comparison of ENDF/B-VI to RPI Results*

Thermal Elastic Cross Sections							
		ENDF			RPI		
Isotope	Abundance	Thermal Elastic	Contribution to Elemental	Percent	Thermal Elastic	Contribution to Elemental	Percent
^{152}Gd	0.200	23.4	0.0468	0.0277	23.4	0.0468	0.0342
^{154}Gd	2.18	7.29	0.159	0.0941	6.69	0.146	0.107
^{155}Gd	14.80	60.8	8.99	5.32	59.7	8.84	6.45
^{156}Gd	20.47	5.64	1.16	0.686	6.93	1.42	1.04
^{157}Gd	15.65	1010	157	92.9	798	125	91.2
^{158}Gd	24.84	3.30	0.820	0.485	3.27	0.812	0.593
^{160}Gd	21.86	3.63	0.795	0.470	3.63	0.794	0.580
Gd	—		169	100.0		137	100.0

*The units of all cross sections are barns. The units of abundance are percent.

the thermal ^{157}Gd resonance (see Table IV). The thermal elastic scattering cross section for ^{157}Gd has a large uncertainty since it is essentially the small difference of two large numbers (total and capture cross sections). Gadolinium-156 also exhibits a large deviation from ENDF in its small and statistically uncertain thermal elastic cross section. Gadolinium-156 has only two resonances below 100 eV. The increase in its thermal elastic cross section is due to the substantial increase in the neutron width of the 80 eV resonance (see Table V). However, the uncertainty on that neutron width (see Table V) encompasses the majority of the increase.

Resonance integrals (Table VIII) are given for each isotope as well as their contribution to the elemental values. The integrations extend from 0.5 eV to 20 MeV. The low-energy cutoff is above the thermal region doublet. The elemental resonance integral for Gd as measured is 2.8% (11 b) larger than that of ENDF. The largest fractional increases in isotopic contributions occur in ^{154}Gd and ^{158}Gd; ^{154}Gd and ^{158}Gd have far fewer resonances than ^{155}Gd or ^{157}Gd. A 14% increase in the ^{158}Gd resonance integral compared to ENDF was measured. This is dominated by the 22.3-eV resonance whose neutron width changed by approximately the same amount.

TABLE VIII

Infinitely Dilute Neutron Capture Resonance Integrals: A Comparison of ENDF/B-VI to RPI Results*

Capture Resonance Integral							
		ENDF			RPI		
Isotope	Abundance	Capture Resonance Integral	Contribution to Elemental	Percent	Capture Resonance Integral	Contribution to Elemental	Percent
^{152}Gd	0.200	476	0.952	0.243	476	0.952	0.237
^{154}Gd	2.18	217	4.73	1.21	261	5.69	1.42
^{155}Gd	14.80	1540	228.	58.3	1570	232	57.7
^{156}Gd	20.47	105	21.5	5.50	104	21.3	5.30
^{157}Gd	15.65	755	118.	30.2	789	123	30.6
^{158}Gd	24.84	62.8	15.6	3.99	71.5	17.8	4.43
^{160}Gd	21.86	7.89	1.72	0.440	7.66	1.68	0.418
Gd	—		391	100		402	100

*The units of all cross sections are barns. The units of abundance are percent.

The resonance integral of ^{154}Gd is 20% larger than that calculated from ENDF resonance parameters. The ^{154}Gd resonance integral is larger than ENDF because of larger widths for resonances at 22.5, 49.63, 65.21, and 76.00 eV (see Table V). Gadolinium-155 contributes more than half of the elemental Gd capture resonance integral, and its contribution is virtually unchanged when compared to that calculated from ENDF parameters.

VII. DISCUSSION: UNCERTAINTIES

In Tables IV and V, estimated uncertainties (on the order of 1σ) are given for the present measurements. They are based upon an envelope of plausible values representing the differences between data sets of equal quality. The sensitivity of the resonance parameters resulting from SAMMY fits to different subsets of the overall data was the method used to estimate the uncertainty on the resultant parameters.

In the thermal region these sensitivity calculations, used to define the uncertainties on resonance parameters in the thermal region, consisted of

1. uncertainty associated with the balance of interactions between ^{155}Gd and ^{157}Gd
2. consistency among natural metal samples of various thicknesses
3. consistency within transmission data within the same experiment
4. uncertainty in capture flux normalization
5. experimental reproducibility of transmission results.

In the epithermal region, uncertainties on resonance parameters include

1. consistency between capture and transmission results
2. stability of radiation widths
3. uncertainty associated with the transmission background
4. Bayesian statistical errors calculated by the SAMMY program.

A detailed discussion of the uncertainty analysis in the present work is given in Ref. 1. The variability of the results is most likely due to systematic errors.

A systematic error is a bias, rather than a random error, and may be due to features that are common to both capture and transmission measurements. The transmission and capture measurements are independent and complementary methods for determining resonance parameters. Features common to both types of experiments and possible sources of systematic uncertainties include using the same electron accelerator, the same neutron-producing target, the same method for determining flight path length, some of the same Gd samples, and some of the same data acquisition electronics. Other potential sources of error include capture flux normalization and the analytical descriptions of the resolution functions.

Uncertainties in sample thicknesses given in Table III are not included in the final uncertainties given in Tables IV and V.

VIII. CONCLUSIONS

Resonance parameters were extracted from combined capture and transmission data sets using the multilevel R-matrix Bayesian code SAMMY. The analysis included Doppler broadening, resolution broadening, and multiple scattering correcting of capture data. Separate resolution functions for transmission and capture were used.

The present measurements assumed the same spin assignments as ENDF for all resonances analyzed.

Neutron widths (Table IV) and thermal (2200 m/s) capture cross sections (Table VI) of the thermal doublet are smaller than currently published (ENDF) values. The neutron widths in particular are significantly smaller than those of ENDF. The thermal (2200 m/s) cross section of ^{157}Gd is 11% smaller than that of ENDF.

In the epithermal region, a great deal of improvement has been made to the Gd resonance parameter database. In the energy region near 96 eV, and particularly above 165 eV, significant changes are suggested to ENDF parameters. New resonances have been suggested where comparisons of data to calculations clearly show they are needed.

Any future gadolinium measurement must be improved beyond the current methods. There were internal inconsistencies between thermal transmission and capture results. There were internal inconsistencies within thermal transmission measurements. The magnitude of these inconsistencies was quantified by the uncertainties on the resonance parameters quoted in Table IV.

Results in the epithermal region could be improved with the use of separated isotopes. Samples would need to be thicker for this region than the samples produced for use in the present measurement in the thermal region. That is, grams of separated isotopes would be needed for epithermal measurements.

REFERENCES

1. G. LEINWEBER, D. P. BARRY, M. J. TRBOVICH, J. A. BURKE, N. J. DRINDAK, H. D. KNOX, R. V. BALLAD, R. C. BLOCK, Y. DANON, and L. I. SEVERNYAK, "Neutron Capture and Transmission Measurements and Resonance Parameter Analysis of Gadolinium," U.S. Department of Energy Office of Scientific and Technical Information (2005).

2. P. F. ROSE and C. L. DUNFORD, "ENDF-102 Data Formats and Procedures for the Evaluated Nuclear Data File ENDF-6," BNL-NCS-44945, Rev. 2, Brookhaven National Laboratory (1997).

3. H. BJERRUM MØLLER, F. J. SHORE, and V. L. SAILOR, "Low-Energy Neutron Resonances in Erbium and Gadolinium," *Nucl. Sci. Eng.*, **8**, 183 (1960).

4. S. F. MUGHABGHAB and R. E. CHRIEN, "S-Wave Neutron Strength Functions of the Gd Isotopes," *Phys. Rev.*, **180**, 1131 (1969).

5. F. B. SIMPSON, "Neutron Resonance Parameters for Sm^{147}, Sm^{149}, Gd^{155}, and Gd^{157}," *Bull. Am. Phys. Soc.*, **2**, 42(NA7) (1957).

6. M. P. FRICKE, W. M. LOPEZ, S. J. FRIESENHAHN, A. D. CARLSON, and D. COSTELLO, "Neutron Resonance Parameters and Radiative Capture Cross Section of Gd from 3 eV to 750 keV," *Nucl. Phys. A*, **146**, 337 (1970).

7. F. RAHN, H. S. CAMARDA, G. HACKEN, W. W. HAVENS, Jr., H. I. LIOU, and J. RAINWATER, "Neutron Resonance Spectroscopy: ^{154,158,160}Gd," *Phys. Rev. C (Nucl. Phys.)*, **10**, 1904 (1974).

8. V. A. ANUFRIEV, S. I. BABICH, and S. M. MASYONOV, EXFOR/CINDA Database, www.nndc.bnl.gov, NNDC CINDA EXFOR Accession #40984 (1987).

9. R. L. MACKLIN, "Neutron Capture Resonances of ^{152}Gd and ^{154}Gd," *Nucl. Sci. Eng.*, **95**, 304 (1987).

10. F. N. BELYAEV, V. P. BOLOTSKIY, B. V. EFIMOV, and G. N. MURADYAN, EXFOR/CINDA Database, www.nndc.bnl.gov, NNDC CINDA EXFOR Accession #41107 (1990).

11. E. N. KARZHAVINA, N. N. PHONG, ad A. B. POPOV, EXFOR/CINDA Database, www.nndc.bnl.gov, NNDC CINDA EXFOR Accession #40162 (1968).

12. E. N. KARZHAVINA, K.-S. SU, and A. B. POPOV, EXFOR/CINDA Database, www.nndc.bnl.gov, NNDC CINDA EXFOR Accession #40405 (1973).

13. M. ASGHAR, P. ASGHAR, E. SILVER, and J. TROCHON, *Nucl. Phys. A*, **145**, 549 (1970).

14. R. E. SLOVACEK, R. C. BLOCK, Y. DANON, C. WERNER, G.-U. YOUK, J. A. BURKE, N. J. DRINDAK, F. FEINER, J. A. HELM, and K. W. SEEMANN, "Neutron Cross Section Measurements at the Rensselaer LINAC," *Proc. Topl. Mtg. Advances in Reactor Physics*, Knoxville, Tennessee, April 11–15, 1994, Vol. II, p. 193, American Nuclear Society (1994).

15. R. C. BLOCK, P. J. MARANO, N. J. DRINDAK, F. FEINER, K. W. SEEMANN, and R. E. SLOVACEK, "A Multiplicity Detector for Accurate Low-Energy Neutron Capture Measurements," *Proc. Int. Conf. Nuclear Data for Science and Technology*, Mito, Japan, May 30–June 3,1988, p. 383.

16. R. C. BLOCK, Y. DANON, R. E. SLOVACEK, C. J. WERNER, G. YOUK, J. A. BURKE, N. J. DRINDAK, F. FEINER, J. A. HELM, J. C. SAYRES, and K. W. SEEMANN, "Neutron Time-of-Flight Measurements at the Rensselaer LINAC," *Proc. Int. Conf. Nuclear Data for Science and Technology*, Gatlinburg, Tennessee, May 9–13, 1994, Vol. 1, p. 81, American Nuclear Society (1994).

17. M. E. OVERBERG, B. E. MORETTI, R. E. SLOVACEK, and R. C. BLOCK, "Photoneutron Target Development for the RPI Linear Accelerator," *Nucl. Instrum. Meth. Phys. Res. A*, **438**, 253 (1999).

18. Y. DANON, R. E. SLOVACEK, and R. C. BLOCK, "The Enhanced Thermal Neutron Target at the RPI LINAC," *Trans. Am. Nucl. Soc.*, **68**, 473 (1993).

19. Y. DANON, R. E. SLOVACEK, and R. C. BLOCK, "Design and Construction of a Thermal Neutron Target for the RPI LINAC," *Nucl. Instrum. Methods Phys. Res. A*, **352**, 596 (1995).

20. E. M. BAUM, H. D. KNOX, and T. R. MILLER, "Chart of the Nuclides," 16th ed., Knolls Atomic Power Laboratory (2002).

21. Y. DANON and R. C. BLOCK, *Nucl. Instrum. Methods Phys. Res. A*, **485**, 585 (2002).

22. G. LEINWEBER, J. A. BURKE, H. D. KNOX, N. J. DRINDAK, D. W. MESH, W. T. HAINES, R. V. BALLAD, R. C. BLOCK, R. E. SLOVACEK, C. J. WERNER, M. J. TRBOVICH, D. P. BARRY, and T. SATO, "Neutron Capture and Transmission Measurements and Resonance Parameter Analysis of Samarium," *Nucl. Sci. Eng.*, **142**, 1 (2002).

23. G. LEINWEBER, J. A. BURKE, C. R. LUBITZ, H. D. KNOX, N. J. DRINDAK, R. C. BLOCK, R. E. SLOVACEK, C. J. WERNER, N. C. FRANCIS, Y. DANON, and B. E. MORETTI, "Neutron Capture and Total Cross Section Measurements and Resonance Parameter Analysis of Zirconium up to 2.5 keV," *Nucl. Sci. Eng.*, **134**, 50 (2000).

24. N. M. LARSON, "Updated Users' Guide for SAMMY: Multilevel R-Matrix Fits to Neutron Data Using Bayes' Equations," ORNL/TM-9179/R5, Lockheed Martin Energy Research Corporation, Oak Ridge National Laboratory (2000).

25. D. B. SYME, "The Black and White-Filter Method for Background Determination in Neutron Time-of-Flight Spectrometry," *Nucl. Instrum. Methods*, **198**, 357 (1982).

26. "MCNP—A General Monte Carlo N-Particle Transport Code, Version 5," LA-UR-03-1987, J. F. BREISMEISTER, Ed., Los Alamos National Laboratory (Apr. 24, 2003).

27. V. McLANE, P. F. ROSE, and C. L. DUNFORD, *Neutron Cross Sections*, Vol. 2, Academic Press, New York (1988).

28. R. E. MacFARLANE and D. W. MUIR, "The NJOY Nuclear Data Processing System Version 91," LA-12740-M, Los Alamos National Laboratory (Oct. 1994).

29. C. COCEVA and M. STEFANON, *Nucl. Phys. A*, **315**, 1 (1979).